Polyethylene terephthalate (PET) micro- and nanoplastic particles affect the mitochondrial efficiency of human brain vascular pericytes without inducing oxidative stress

Sean M. Gettings [a], William Timbury [a], Anna Dmochowska [b], Riddhi Sharma [a], Rebecca McGonigle [c], Lewis E. MacKenzie [c], Guillaume Miquelard-Garnier [b], Nora Bourbia [a,*]

[a] UK Health Security Agency, Radiation Effects Department, Radiation Protection Science Division, Harwell Science Campus, Didcot, Oxfordshire OX11 0RQ, UK
[b] Laboratoire PIMM, CNRS, Arts et Métiers Institute of Technology, Cnam, HESAM Universite, 75013 Paris, France
[c] Department of Pure and Applied Chemistry, University of Strathclyde, Glasgow G1 1RD, UK

ARTICLE INFO

Keywords:
Nanoplastic
Microplastic
Pericytes
Oxidative stress
Mitochondria
PET
Polyethylene terephthalate

ABSTRACT

The objective of this investigation was to evaluate the influence of micro- and nanoplastic particles composed of polyethylene terephthalate (PET), a significant contributor to plastic pollution, on human brain vascular pericytes. Specifically, we delved into their impact on mitochondrial functionality, oxidative stress, and the expression of genes associated with oxidative stress, ferroptosis and mitochondrial functions. Our findings demonstrate that the exposure of a monoculture of human brain vascular pericytes to PET particles in vitro at a concentration of 50 μg/ml for a duration of 3, 6 and 10 days did not elicit oxidative stress. Notably, we observed a reduction in various aspects of mitochondrial respiration, including maximal respiration, spare respiratory capacity, and ATP production in pericytes subjected to PET particles for 3 days, with a mitochondrial function recovery at 6 and 10 days. Furthermore, there were no statistically significant alterations in mitochondrial DNA copy number, or in the expression of genes linked to oxidative stress and ferroptosis, but an increase of the expression of the gene mitochondrial transcription factor A (*TFAM*) was noted at 3 days exposure.

These outcomes suggest that, at a concentration of 50 μg/ml, PET particles do not induce oxidative stress in human brain vascular pericytes. Instead, at 3 days exposure, PET exposure impairs mitochondrial functions, but this is recovered at 6-day exposure. This seems to indicate a potential mitochondrial hormesis response (mitohormesis) is incited, involving the gene *TFAM*. Further investigations are warranted to explore the stages of mitohormesis and the potential consequences of plastics on the integrity of the blood-brain barrier and intercellular interactions. This research contributes to our comprehension of the potential repercussions of nanoplastic pollution on human health and underscores the imperative need for ongoing examinations into the exposure to plastic particles.

1. Introduction

Nanoplastics (plastic particles <1000 nm) and microplastics (plastic particles <1000 μm) are posing a health threat as they are polluting our environment (Landrigan et al., 2020; Zhang et al., 2021) and food (Liu et al., 2021) to the point of finding plastic particles in human blood (Leslie et al., 2022), lung (Jenner et al., 2022), placenta (Ragusa et al., 2021), heart (Yang et al., 2023), and breast milk (Ragusa et al., 2022). Plastic particles are also released from plastic packaging (Jadhav et al., 2021). For instance, it has been estimated that microwaving plastic containers for three minutes could release about 4 million microplastics and about 2 billion nanoplastic particles from one square centimetre of plastic (Hussain et al., 2023). The same authors estimated the highest daily intake of plastic particles from microwaved water or dairy products in plastic containers alone represents about 20 ng/kg per day for toddlers consuming microwaved dairy products from polypropylene containers.

Studies on the effect of nanoplastics on brain and blood-brain barrier (BBB) functions are still limited (Prüst et al., 2020) but it is established that plastic particles cross the blood-brain barrier and can be transferred

* Corresponding author.
E-mail address: nora.bourbia@ukhsa.gov.uk (N. Bourbia).

through the food chain (Kopatz et al., 2023; Mattsson et al., 2017). Additionally, nanoplastics can be carriers for other molecules that may enhance their accumulation inside the brain (Chen et al., 2017). Plastic particles can also induce oxidative stress (Lei et al., 2018; Schirinzi et al., 2017), mitochondrial dysfunction (Murali et al., 2015), and affect the expression of genes linked to neurodevelopment in a 3-dimensional model of human embryonic stem cells. This included genes associated with neurogenesis regulation and telencephalon differentiation (Hoelting et al., 2013).

Pericyte cells are fundamental constituents of the blood-brain barrier and have several critical functions such as maintaining the blood-brain barrier and clearing toxins (Bell et al., 2010; Quaegebeur et al., 2010). Dysfunction in these cells is associated with neurodegenerative diseases such as Alzheimer's and Parkinson's diseases (Baloyannis and Baloyannis, 2012; Halliday et al., 2016; Lendahl et al., 2019; Quaegebeur et al., 2010; Winkler et al., 2014), which are multifactorial diseases where environmental pollutants, such as neurotoxic metals, metal-nanoparticles, and pesticides, are implicated as known risk factors (Chin-Chan et al., 2015; Kriit et al., 2021). Therefore, it is important to assess whether nano- and microplastic particles can interfere with pericyte bioenergetics, hindering their neuroprotective functions.

To study potential adverse effects of plastic particle exposure on pericytes, we made our own polyethylene terephthalate (PET) plastic particles. PET was selected as the plastic feed stock because it is widely used for food containers and drink bottles. Also, containers made of PET release more plastic than those made of polypropylene (Hussain et al., 2023). In the study design, we confirmed the composition of PET particles using Fourier-transform infrared spectroscopy (FTIR), thermogravimetric analysis (TGA), and differential scanning calorimetry (DSC). Additionally, the concentration of plastic micro/nano particles is a key variable. We used a concentration of 50 μg/ml which is 31.25 times higher than the average plastic particle detected in human blood (Leslie et al., 2022) to take in account potential bioaccumulation at the BBB (Shih et al., 2018) and occupational exposures (Salthammer, 2022).

Finally, we simulated a chronic exposure by exposing human brain vascular pericytes (HBVP) cultured in vitro to PET particles for 3, 6 and 10 days and assessed whether PET particles can induce oxidative stress, mitochondrial dysfunctions, and eventually ferroptotic cell death.

2. Materials and methods

2.1. Plastic particle characterisation

2.1.1. Plastic particle generation

Realistic plastic particles were generated based on the protocol developed by Ji et al., 2020 with the adaptations as follows. Micro- and nanoplastic particles were generated from polyethylene terephthalate (PET) confectionary-style plastic jars purchased from a scientific supply retailer (cat: 129–0590; VWR International). These jars were selected as they can be readily purchased by other researchers to aid in comparative studies. The jars were then shredded using a hole-puncher to generate feed material (~4 mm diameter). The PET feed material was ground in a Pulverisette 2 automatic pestle, from the manufacturer Fritsch, for 4 h. The automatic pestle was cooled with dry ice (which was added every 15 min). The PET plastic was then placed in 7 ml steel tubes with 10 × 2 mm steel ball bearings to be broken down further with the Precellys Evolution Touch tissue homogeniser with the Cryolys Evolution attachment. The tubes containing PET were then purged with liquid nitrogen for 12 min before agitation in the Cyrolys Precellys at two cycles of 10,000 RPM for 60 s with a 20 s rest between cycles. This was repeated 5 times. The resulting PET micro- and nanoplastic mix was sieved from the remaining feed material using Wstyler brass sieves (No.60) down to a 250 μm tolerance. A stock concentration of 10 mg/ml PET with a particle size range of 82 nm (determined using SEM, see section 2.1.2) to 250 μm was added to 0.05% bovine serum albumin (BSA) (cat: A9647-10G; Merck) and pure, sterile water (cat: AM9937, Invitrogen) to facilitate the suspension and dispersal of PET particles.

2.1.2. Plastic particle sizing

For scanning transmission electron microscopy (STEM) and scanning electron microscopy (SEM) imaging, a fresh grid (holey carbon film on 200 mesh, AGS147H, Agar Scientific Ltd) was gripped using tweezers and immersed within a freshly agitated particle solution. The grid was then air dried and then mounted on a copper grid holder and affixed with quick drying conductive silver paint (AGG302, Agar Scientific Ltd). Imaging was conducted using a variable pressure field emission gun scanning electron microscope (FEI Quanta 250), operating in high vacuum mode with an accelerating voltage of 30 kV and at 100,000× magnification. STEM imaging was conducted via a two-segment solid-state detector holder operating in bright-field mode and mounted under the sample. SEM imaging was conducted using the standard secondary electron (SE) detector. Images were saved in uncompressed .TIF format at a resolution of 1024 × 943 pixels. Nanoparticle diameters were measured manually from SEM images by using ImageJ software (Schneider et al., 2012).

2.1.3. Plastic particle characterisation

Dynamic light scattering (DLS) was used to determine the size distribution and polydispersity index (PDI) of plastic particle samples. These measurements were carried out using a Malvern Zetasizer Nano Zs ZEN3600 instrument. The zeta potential was measured using the same instrument via a folded capillary zeta cell. The 0.05% BSA:water solution, 10 mg/ml stock PET particles:0.05% BSA mixture (particle size <250 μm), and 1 mg/ml PET particles:0.05% BSA mixture were filtered through a 0.45 μm syringe filter. All samples were sonicated for 30 mins via a sonic bath prior to measurement with any sediment present after sonication excluded from analysis.

The chemical composition of PET particles was evaluated by Fourier-transform infrared spectroscopy (FTIR). The sample was ground, mixed with dried spectroscopic grade potassium bromide, and formed into a pellet using a laboratory press. The mass of PET particles was equal to 1 wt% of the pellet. The spectrum was recorded on a Frontier spectrometer (Perkin Elmer) in the range of 4000–650 cm^{-1} at 2 cm^{-1} resolution and is an average of 32 scans.

Thermal stability of the sample was determined by thermogravimetric analysis (TGA) in the range of 25–600 °C with a 10 deg./min heating rate (Q50, TA Instruments). The experiment was conducted under nitrogen atmosphere (50 ml/min) in a platinum crucible with a sample mass of about 7 mg.

Thermal phase transitions of the PET particles were analyzed by differential scanning calorimetry (DSC) in the range of 30–325 °C at 10 deg./min heating rate (Q1000, TA Instruments). Two heating cycles were applied in order to erase the thermomechanical history of the material. The measurement was performed under nitrogen flow (50 ml/min) in a sealed aluminum pan with the sample mass of about 3 mg.

2.2. Cell culture

Human Brain Vascular Pericytes (HBVP) (cat.: 1200; ScienCell) were cultured in Pericyte Medium (PM, Cat. #1201-b; ScienCell) supplemented with pericyte growth supplement (cat. #1252; ScienCell), 2% foetal bovine serum (FBS) and 1% Penicillin-Streptomycin, and were kept in an incubator at 37 °C and 5% CO_2. Cells were initially seeded at 1×10^6 cells in T75 flasks (growth medium volume of 20 ml) to then be seeded at 30,000 cells per well in 96 well plates (growth medium volume of 100 μl per well) and in Seahorse cartridges (growth medium volume of 80 μl per well), or at 0.25×10^6 in T25 (growth medium volume of 5 ml). At confluency 60–70%, pericyte cells were exposed to either a final concentration of 50 μg/ml PET (< 250 μm in size, BSA final concentration of 0.0001%) or the control medium (supplemented pericyte medium mentioned above, adjusted to 0.0001% BSA) used for PET dilution for 3, 6 and 10 days. At 3-, 6- or 10-days cells were processed for

further experiment. Cells used for protein, DNA or RNA extractions were rinsed with Dulbecco's phosphate-buffered saline (DPBS) (cat: 14040174, ThermoFisher), trypsinised (cat: T4174–100 ml, Merck) and the trypsin was neutralised using pericyte medium supplemented as mentioned above. The cells were then centrifuged at 1000 *g*, and the cell pellets collected for further experiments.

2.3. Cell counting assay

Cell counting assay was performed using the Cell Counting Kit 8 (cat: ab228554, Abcam) as per manufacturer manual, by adding 10 µl per well of the WST-8 solution to cells cultured in 96 well plates followed by an incubation time of 2 h at 37 °C and 5% CO_2 before absorbance reading. Cultured pericytes were exposed to PET at 50 µg/ml or control medium for 3, 6 and 10 days. Absorbance readings for the experimental groups were blanked to wells with media only, either PET or control medium. Unpaired *t*-test or Mann-Whitney test were used to compare experimental groups.

2.4. Mitochondrial functions

2.4.1. Seahorse XF cell mito stress test

To assess the mitochondrial respiration, a mitochondrial stress test was performed using the Agilent Seahorse XFp analyzer (Fig. 1). The manufacturer protocol was followed using Seahorse XF Cell Mito Stress Test Kit (cat.: 103010–100; Agilent), Seahorse XFp FluxPak (103022–100; Agilent), and the Seahorse XF DMEM assay medium pack (103680–100; Agilent). Cell density of 30,000 cells per well, and drug concentrations (Oligomycin at 1.5 µM, Carbonyl cyanide-4 (trifluoromethoxy) phenylhydrazone at 0.5 µM, and rotenone/antimycin A at 0.5 µM) were determined and optimised for the HBVP cells prior to the experiment. Oxygen consumption rate (OCR) expressed in pmol/min is used to assess each aspect output (basal respiration, ATP production, proton leak, maximal respiration, non-mitochondrial respiration, and spare capacity) of the Seahorse XF Cell Mito Stress. The coupling efficiency expressed as a percentage, and the extracellular acidification (ECAR) is expressed in mpH/min. Non-mitochondrial oxygen consumption (NMOC) represents the minimum rate measurement following the application of rotenone. Basal respiration refers to the sum of NMOC subtracted from the last rate measurement prior to the application of oligomycin. Similarly, the maximal respiration rate refers to the sum of NMOC subtracted from the maximum respiration rate measurement following the application of FCCP (Carbonyl cyanide-*p*-trifluoromethoxyphenylhydrazone). The proton (H^+) pump leak is defined as minimum rate measured following the application of oligomycin less the NMOC. ATP production is determined by subtracting the minimum rate measured following the application of oligomycin from the final rate measurement prior to the application of oligomycin. The spare respiratory capacity is determined through subtracting the basal respiration from the maximal respiration. The coupling efficiency (%) is equal to the ATP production rate divided by the basal respiration rate multiplied by 100 to form a percentage.

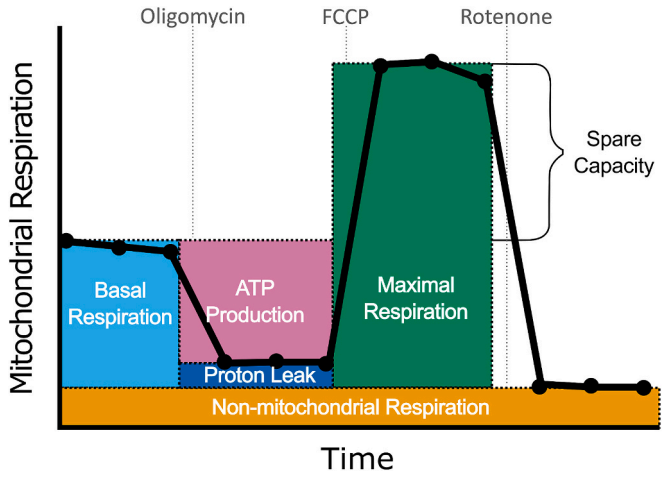

Fig. 1. Agilent Seahorse XF Cell Mito Stress Test showing the mitochondrial functions assessed.

Mixed-effects analysis was used to compare OCR and ECAR and unpaired *t*-test or Mann-Whitney test was used to compare all other mitochondrial function outputs between experimental groups ($n = 5$ or 6 per group). Experimental groups were randomly assigned to the wells of the Seahorse cartridge.

2.4.2. Relative mitochondrial DNA copy

To determine relative mitochondrial DNA copies of pericytes after exposure to plastic particles, DNA was extracted by applying DNeasy Blood & Tissue Kit (cat.: 69504; Qiagen) to the pelleted cells, followed by quantitative polymerase chain reaction (qPCR) using PerfeCTa SYBR Green SuperMix (cat.: 733–1246; VWR International) for an initial 95 °C for 10 min followed by 40 cycles (95 °C for 15 s, followed by 62 °C for 60 s, and then 72 °C for 20 s) in a Magnetic Induction Cycler (Mic qPCR, Bio Molecular Systems).

The primer set of the nuclear DNA was selected to target the gene *B2M* (alias *Beta-2-Microglobulin*) (Forward sequence: 5' TGCTGTCTCCATGTTTGATGTATCT 3'; Reverse sequence: 5' TCTCTGCTCCCCACCTCTAAGT 3'; the amplicon size is 86 base pairs) and the primer set for the mitochondrial DNA was selected to target the gene *MT-TL1* (alias *TRNA-Leu (UUR)*) (Forward sequence: 5' CACCCAAGAACAGGGTTTGT 3'; Reverse sequence: 5' TGGCCATGGGTATGTTGTTA 3'; the amplicon size is 107 base pairs). Both set of primers have been validated for their efficiency prior experiment by testing a standard curve of each primer pairs using a 1:3 serial dilution of pericyte DNA. The relative mitochondrial DNA content was determined as the formula $2 \times 2^{\Delta CT}$, where ΔCT = nuclear DNA CT – mitochondrial DNA CT (Rooney et al., 2015). Unpaired *t*-test was used to compare both experimental groups ($n = 4$ per group).

2.5. Oxidative stress responses and ferroptosis

2.5.1. Oxidative stress assay

The presence of reactive oxygen species (ROS) was assessed using the general oxidative stress indicator CM-H2DCFDA (cat: C6827, ThermoFisher Scientific). As per the manufacturer's protocol, the CM-H2DCFDA probe was initially reconstituted in dimethyl sulfoxide (DMSO) (cat: 317275, Sigma-Aldrich) and then further dilutions were carried out using PM to achieve a final concentration of 5 µM. Cells were washed using 100 µl HBSS (cat: 15266355, Thermo Fisher Scientific) per well of a 96 well plate, then given 100 µl of the PM supplemented with the probe for a 15 min incubation period. After which, the cells were washed with HBSS three times. 100 µl of HBSS were added to all wells, positive control wells received the addition of 2 µl of hydrogen peroxide (cat: 101284 N, VWR International) to achieve a final concentration of 0.5%, giving a final molarity of 0.163 M. Reading of the 96 well-plate was done on a spectrophotometer at 485/528 nm excitation/emission readings for the experimental groups were blank to wells with media only. Kruskal-Wallis (KW) test or Mann-Whitney (MW) test was used to compare both experimental groups.

2.5.2. Expression of genes associated with oxidative stress, ferroptosis, and mitochondrial functions

Reverse transcription quantitative polymerase chain reaction (RT-qPCR) was used to assess whether the PET particles had an impact on the expression of the genes associated with oxidative stress, ferroptosis, and mitochondrial functions. RNA extraction of the pelleted cells was done using RiboPure™ RNA Purification Kit (cat.: AM1924; Thermo Fisher Scientific) followed by a cDNA conversion using High-Capacity cDNA

Reverse Transcription kit (cat.: 4368814; Thermo Fisher Scientific). RT-qPCR was performed using PerfeCTa SYBR Green SuperMix with the equipment Mic qPCR for initial 90 °C for 2 min followed by 40 cycles (95 °C for 5 s, followed by 58 °C for 15 s, and then 72 °C for 10 s). All set of primers (Table 1) were previously validated for their efficiency in prior experiments by testing a standard curve of each primer pairs using a 1:3 serial dilution of pericyte cDNA. The gene beta-2-microglobulin (*B2M*) is used as the housekeeping gene to determine the delta cycle threshold (ΔCT) which was then used to perform statistical analysis to compare both experimental groups. Unpaired *t*-test or Mann-Whitney test were to compare experimental groups ($n = 5$ to 6 per group, rt-qPCR was performed in triplicate).

2.6. Statistics

Normality distribution between samples was tested using the Shapiro-Wilk test. The Mann-Whitney *U* test and Kruskal-Wallis test were used for non-parametric comparison between experimental groups, and the two-tailed unpaired t-test was used when comparing experimental groups with a normal distribution, with Welch's correction when both populations have unequal variance. The Mixed-effects model was used for repeated measures multiple comparisons between both experimental groups in place of ANOVA as not all groups number of data values. All statistical analysis has been performed using the software GraphPad Prism 9.4.0 and all figures were formatted in Inkscape *V*.1.1.2.

3. Results

3.1. Plastics characterisation

From electron microscopy (Fig. 2A-F), the average diameter of the PET particles observed was determined to be 205 ± 79 nm (diameter ± std. deviation; $n = 60$) with a particle size ranging from 82 nm to 385 nm (not including aggregates). Microplastics were observed in the medium however it was apparent they did not adhere well to the sample grid because few plastic particles were observed under electron microscopy. Therefore, electron microscopy measurements are unlikely to be exactly representative of the plastic particle population. However, these electron microscopy images confirmed that the 10 mg/mL PET stock contains nanoparticles (nanoparticles are defined as particles <1000 nm) (Hartmann et al., 2019). Additional optical microscopy images were obtained of the pericyte medium containing 50 μg/mL PET in a 96 well plate placed inside the Incucyte S3 live cell imager. These optical microscopy images (Fig. 2G and H) demonstrate the presence of larger PET particles or aggregates of smaller PET particles. Nanoplastic particles will be present in these images too however are below the diffraction limit of optical microscopy (i.e. ~250 nm) (Heintzmann and Ficz, 2006) and therefore will not be apparent.

The DLS measurement of plastic particles shows bimodal size distributions (d.nm) corresponding to two peaks (Peak 1 and Peak 2, Table 2) observed. This confirms a bimodal distribution of individual and aggregated nanoplastic populations indicated by electron microscopy (see Fig. 2). The polydispersity index (PDI, Table 2) decreases following filtration of the plastic particles as expected as the size distribution is reduced. The zeta potential (Table 2) of the BSA 0.05% medium exhibited a modest negative charge (−9.7 mV) whereas plastic particles exhibited a greater negative charge (−44.2 ± 6.9 and − 22.1 ± 6.4 mV) for the non-filtered and filtered particles respectively. This difference in zeta potential between both plastic particle samples could be attributed to the different size fractions because – as seen in Fig. 2 - larger particles will be non-uniform agglomerates (also evidenced by high PDI), and which will therefore present an altered surface area compared to smaller and more uniform filtered particles (evidenced by lower PDI). This may indicate a limitation of zeta potential and DLS analysis of plastic particles.

The FTIR results clearly confirm that PET particles were composed of PET and that they had undetectable level of impurities because only peaks correlated with the structure of PET were observed in the spectrum (Fig. 3A). The peak at 2970 cm^{-1} was attributed to C—H stretching vibrations (Fávaro et al., 2007). Carbonyl stretching band can be seen at 1717 cm^{-1}, corresponding to C═O stretching. Skeletal stretching vibrations were observed at 1410 cm^{-1}. The peak at 1344 cm^{-1} corresponded to $–CH_2$ wagging in trans conformation (Andanson and Kazarian, 2008). Three different vibrations can be seen at 1244 cm^{-1}, namely the stretching of C(—O)O, stretching of ring-ester C—C, and in-plane bending of C—O (Donelli et al., 2009). The peaks at 1122 and 1098 cm^{-1} were correlated with C—O stretching. This doublet is linked with the crystallinity of PET. The higher the intensity of the peak at 1122 cm^{-1}, the bigger the amount of the crystalline phase. The band at 1011 cm^{-1} indicated the in-plane vibrations of benzene. Finally, the out-of-plane benzene group vibrations were observed at 871 and 723 cm^{-1}. FTIR of the PET bottle (Fig. 3A) shows some peaks have a lower intensity than the PET particles suggesting the possible addition of other matter during the processing of PET for this study. This result confirms that there is an extremely low quantity of additives are present in the obtained nanoparticles.

To confirm that, the thermal stability of the sample can be examined. The TGA results show a single step of the sample decomposition, indicating again that no significant amount of additives is detected (Fig. 3B) (Han et al., 2018). The degradation started at the onset temperature (T_o) equal to 411 °C, with the maximum rate at 439 °C, as indicated by the peak of the derivative thermogravimetric (dTG) curve. The residual mass was equal to 13%, which in the case of the measurement performed in nitrogen atmosphere is attributed to the char. TGA results shows a 3.8% residual mass that did not decompose in the PET particles compared to stock PET bottle and a consistent rate of mass loss with increasing temperature (Fig. 3B), again supporting a very low fraction of

Table 1
List of rt-qPCR primer sequences.

Genes	Forward primers sequences (5′-3′)	Reverse primers sequences (5′-3′)
B2M	TGCTGTCTCCATGTTTGATGTATCT	TCTCTGCTCCCCACCTCTAAGT
NOTCH3	GAACTCCTCTCCCCCTGCACC	CCAGGTTGGTGCAGATACCATGA
SOD1	GGTGGGCCAAAGGATGAAGAG	CCACAAGCCAAACGACTTCC
HIF1α	ATGCTTTAACTTTGCTGGCCCC	GCT TTGGCGTTTCAGCGGT
GXP4	GAGGCAAGACCGAAGTAAACTAC	CCGAACTGGTTACACGGGAA
SLC7A11	TCTCCAAAGGAGGTTACCTGC	AGACTCCCCTCAGTAAAGTGAC
NCOA4	GAGGTGTAGTGATGCACGGAG	GACGGCTTATGCAACTGTGAA
KEAP1	CTGGAGGATCATACCAAGCAGG	GGATACCCTCAATGGACACCAC
MNF1	TGT TTTGGTCGCAAACTCTG	CTGTCTGCGTACGTCTTCCA
MNF2	ATGCATCCCCACTTAAGCAC	CCAGAGGGCAGAACTTTGTC
PPARGC1A	TCTGAGTCTGTATGGAGTGACAT	CCAAGTCGTTCACATCTAGTTCA
NRF1	GGTGCAGCACCTTTGGAGAA	CCAGAGCAGACTCCAGGTCTTC
TFAM	ATGGCGTTTCTCCGAAGCAT	TCCGCCCTATAAGCATCTTGA
PINK1	CCCAAGCAACTAGCCCCTC	GGCAGCACATCAGGGTAGTC

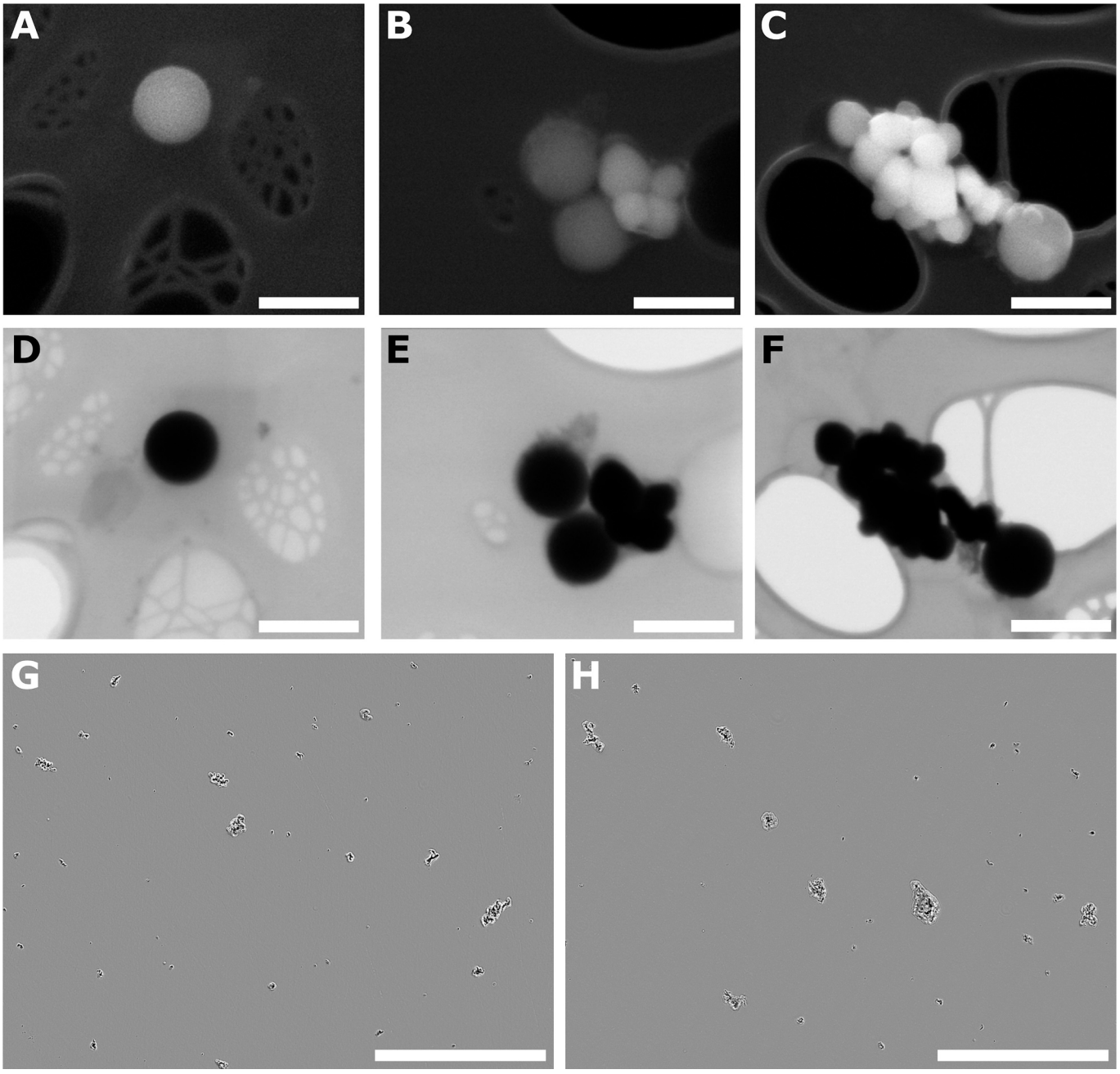

Fig. 2. Representative SEM (top row; A, B and C), STEM (bottom row; D, E and F), and optical microscopy (G, H) PET images of plastic particles used in this study. Scale bar in A to F represents 400 nm, and in G and H represents 200 μm. SEM more clearly shows the morphology of individual and agglomerated nanoplastics and optical microscopy more clearly shows agglomerate of microplastics.

Table 2
Dynamic light scattering and Zeta potential.

Sample	Zeta (mV)	Size (d.nm) Peak 1	Size (d.nm) Peak 2	PDI
BSA 0.05%	−9.7 ± 4.0	8 ± 2	134 ± 37	0.26
10 mg/ml plastic particles	−44.2 ± 6.9	84 ± 12	945 ± 194	0.71
1 mg/ml plastic particles (filtered at 0.45 μm)	−22.1 ± 6.4	6 ± 1	120 ± 33	0.33

non-PET material.

The DSC results of the fabricated PET particles show a typical for PET behavior during the 1st heating with a glass transition at 86 °C and an endothermic peak corresponding to melting at 247 °C (Fig. 3C)(Antoniadis et al., 2011). Then, during cooling, an exothermic peak correlated with crystallization is observed at 192 °C. The peak is sharp at the higher temperature, but there is a slight shoulder at 182 °C, indicating the crystallization of a different population, such as chains with a different molecular weight. The glass transition is noted at 76 °C. Finally, during the 2nd heating, the glass transition can be seen at 82 °C, followed by a bimodal melting peak with the maxima, at 237 and 244 °C. DSC results of PET bottle (Fig. 3C) before processing shows consistent 1st heat, cooling and 2nd heating curves suggesting the preservation of crystalline structure in the PET particles. These data suggest PET particles were

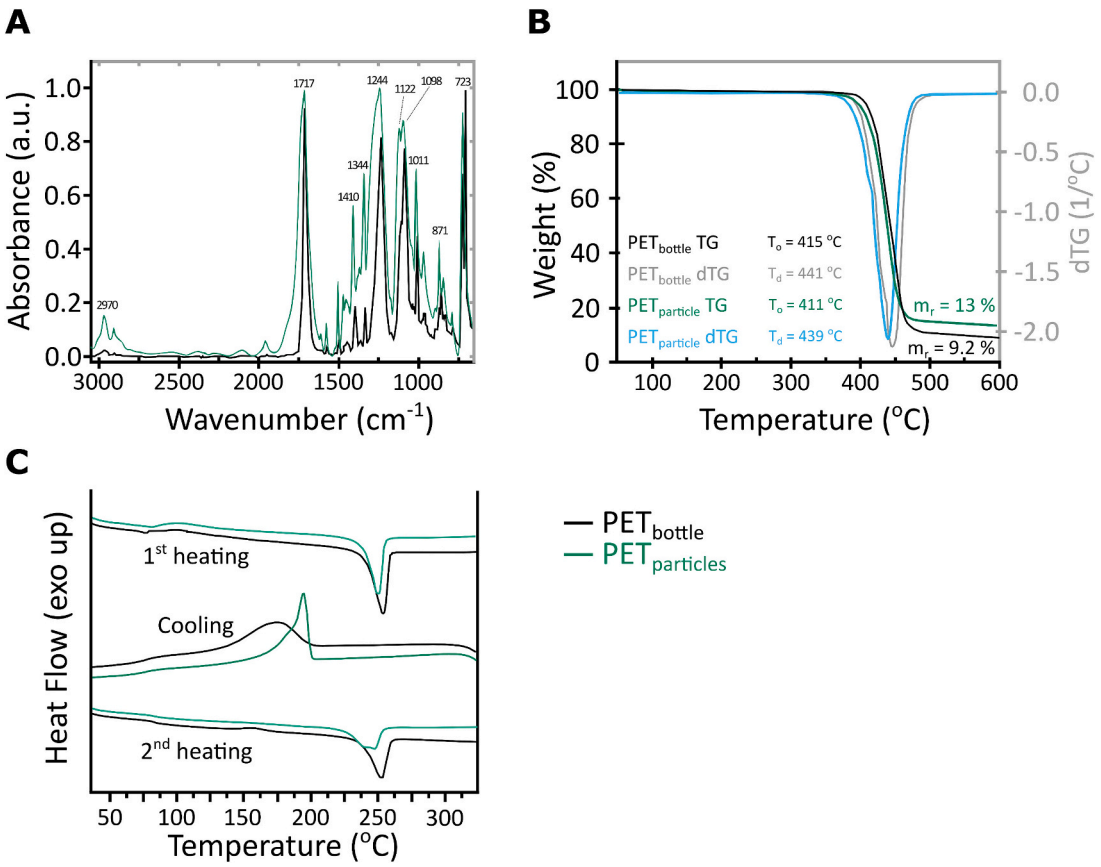

Fig. 3. Characterisation of PET plastic bottle and derived particles: FTIR spectrum of PET bottle and fabricated PET particles with marked wavenumbers of the peaks of interest (A). TG (PET_{bottle}; black, $PET_{particle}$; green) and dTG (PET_{bottle}; grey, $PET_{particle}$; blue) thermograms of PET particles (B). DSC thermogram of PET bottle (black) and particles (green) (C) with representation of the 1st heating, cooling, and 2nd heating stages. (For interpretation of the references to colour in this figure legend, the reader is referred to the web version of this article.)

composed of two different crystalline phases, possibly due to a bimodal distribution of the polymer chains' molecular weights.

3.2. Cell viability

Cell counting assay was performed for pericyte exposed to PET for 3, 6 and 10 days. There is a no change of absorbance intensity of pericytes suggesting no change in cell viability following 3 days ($P = 0.5497$, $n = 24$ per group), 6 days ($P = 0.9904$, $F(22,22) = 1.987$, $n = 23$ per group), and 10 days ($P = 0.1081$, $F(23,23) = 1.045$, $n = 24$ per group) treatment of PET at 50 μg/ml.

3.3. Oxygen consumption rate (OCR) and extracellular acidification (ECAR)

The Agilent Seahorse XFp Mito Stress Test was used to assess different bioenergetic measures of the mitochondrial respiration. The Mito Stress Test measures the OCR expressed in pmol/min and ECAR expressed in mpH/min.

PET exposure to cells did not affect the ECAR compared to the control independently to the exposure time, despite observing an interaction between time and exposure treatment at 3 days exposure (Treatment: $P = 0.1786$, $F(1,10) = 2.093$; Time: $P < 0.0001$, $F(2.315, 23.15) = 292.3$; Interaction Time x Treatment: $P < 0.0001$, $F(11,110) = 7.459$, Fig. 4A), nor at 6 days (Treatment: $P = 0.1457$, $F(1,10) = 2.489$; Time: $P < 0.0001$, $F(1.927, 19.27) = 306.8$; Interaction Time x Treatment: $P = 0.2370$, $F(11, 110) = 1.295$, Fig. 4B) or 10 days exposure (Treatment: $P = 0.2207$, $F(1, 9) = 1.732$; Time: $P < 0.0001$, $F(1.556, 14.00) = 112.9$; Interaction Time x Treatment: $P = 0.1279$, $F(11, 99) = 1.544$, Fig. 4C).

However, PET significantly decreased the OCR when cells are exposure to PET for 3 days (Treatment: $P = 0.0008$, $F(1, 10) = 22.79$; Time: $P < 0.0001$, $F(1.199, 11.99) = 403.7$; Interaction Time x Treatment: $P < 0.0001$, $F(11, 110) = 16.40$, Fig. 4D), yet no treatment significant changed was observed when the pericytes are exposed to PET for 6 days (Treatment: $P = 0.1457$, $F(1, 10) = 2.489$; Time: $P < 0.0001$, $F(1.927, 19.27) = 306.8 = 403.7$; Interaction Time x Treatment: $P = 0.2370$, $F(11, 110) = 1.295$, Fig. 4E) and 10 days (Treatment: $P = 0.2207$, $F(1, 9) = 1.732$; Time: $P < 0.0001$, $F(1.556, 14.00) = 112.9$; Interaction Time x Treatment: $P = 0.1279$, $F(11, 99) = 1.544$, Fig. 4F).

At day 3 exposure to PET, pericytes do not show a difference in proton leak ($P = 0.4134$, $F(5,5) = 1.612$, Fig. 5A), expressed in pmol per ml, or coupling efficiency ($P = 0.4027$, $F(5,5) = 1.496$, Fig. 5B), expressed in percentage, compared to the control group.

However, the non-mitochondrial oxygen consumption ($P = 0.018$, $F(5,5) = 1.680$, Fig. 6A), the basal respiration ($P = 0.0019$, $F(5,5) = 2.475$, Fig. 6B), the maximal respiration ($P = 0.0012$, $F(5,5) = 1.120$, Fig. 6C), the ATP production ($P = 0.0007$, $F(5,5) = 3.427$, Fig. 6D) and the spare respiratory capacity ($P = 0.0017$, $F(5,5) = 1.045$, Fig. 6E) – all expressed in pmol per ml – are significantly decreased in pericytes exposed to PET for 3 days compared to the control group.

At day 6 exposure, the pericytes do not show significant differences in non-mitochondrial oxygen consumption ($P = 0.1536$, $F(5,5) = 1.315$, Fig. 6A), maximal respiration ($P = 0.2837$, $F(5,5) = 1.787$, Fig. 6C), spare respiratory capacity ($P = 0.4367$, $F(5.5) = 1.654$, Fig. 6E), proton leak ($P = 0.4185$, $F(5,5) = 3.715$, Fig. 5A), and coupling activity ($P = 0.8773$, $F(5.5) = 4.014$, Fig. 5B) when exposed to PET compared to the control group.

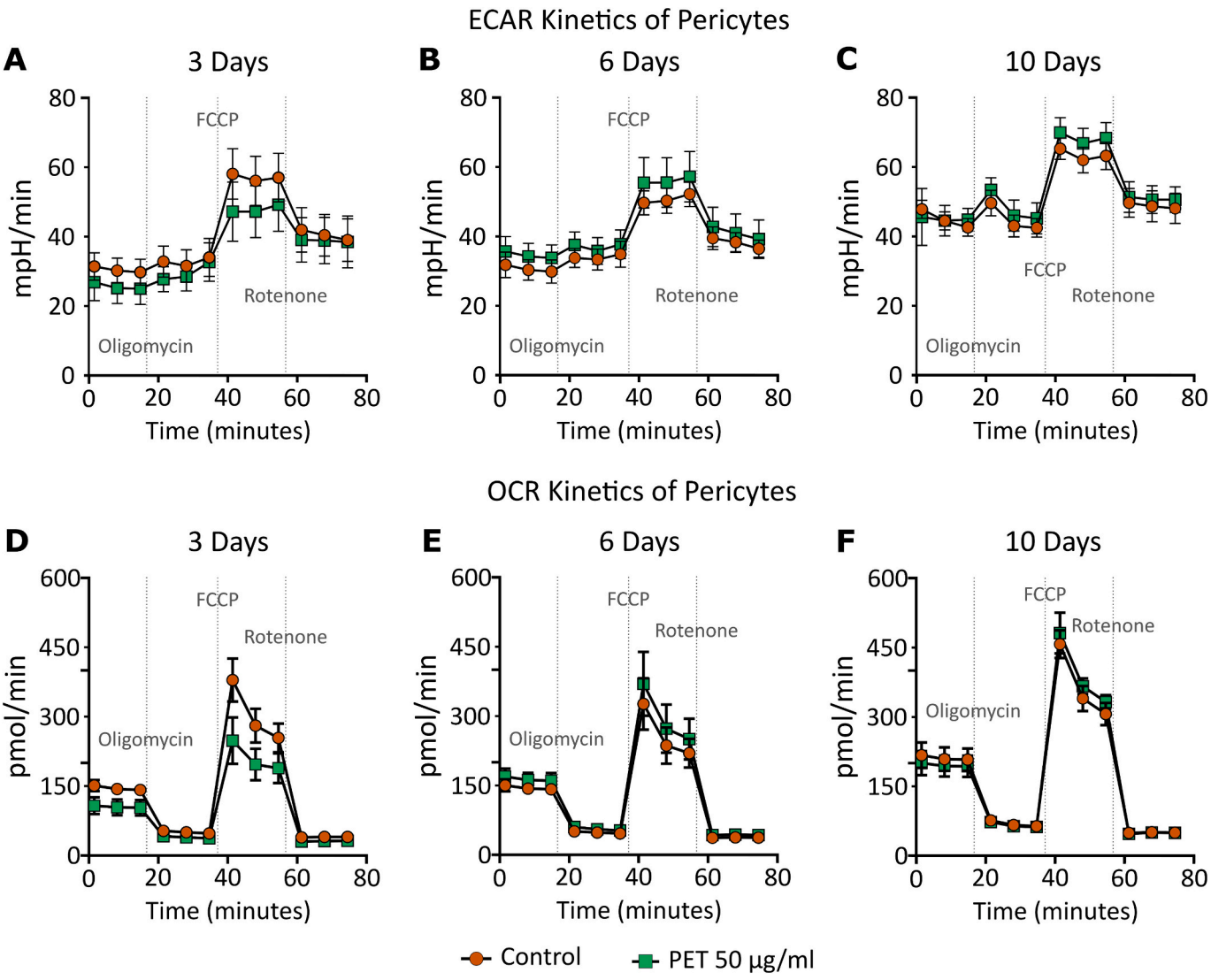

Fig. 4. Extracellular acidification rate (ECAR, A) and oxygen consumption rate (OCR, B) kinetics: ECAR and OCR of pericytes exposed to control (round orange) or 50 µg/ml PET (square green) for 3, 6 and 10 days. (For interpretation of the references to colour in this figure legend, the reader is referred to the web version of this article.)

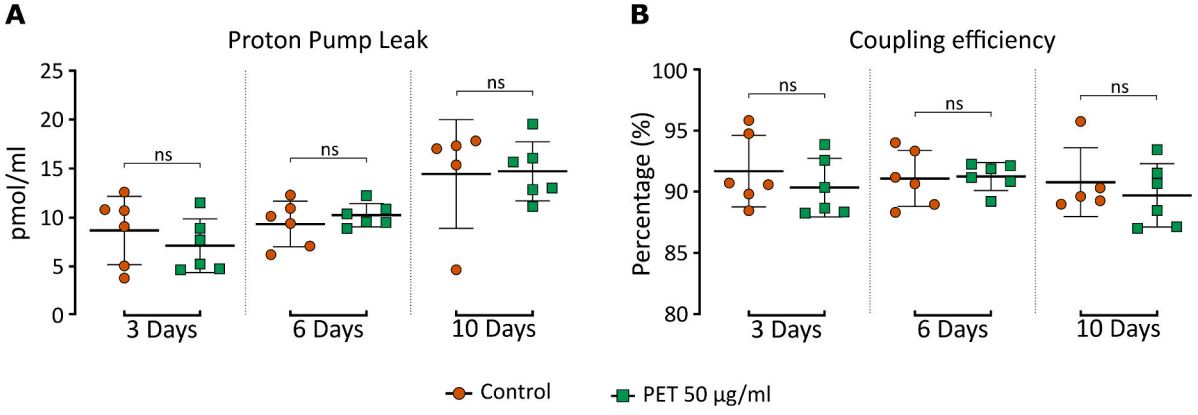

Fig. 5. Proton leak (A), and coupling efficiency (B) activity. Control (round orange) and 50 µg/ml PET (square green) exposure for 3, 6 and 10 days on pericytes. ns = non-significant. (For interpretation of the references to colour in this figure legend, the reader is referred to the web version of this article.)

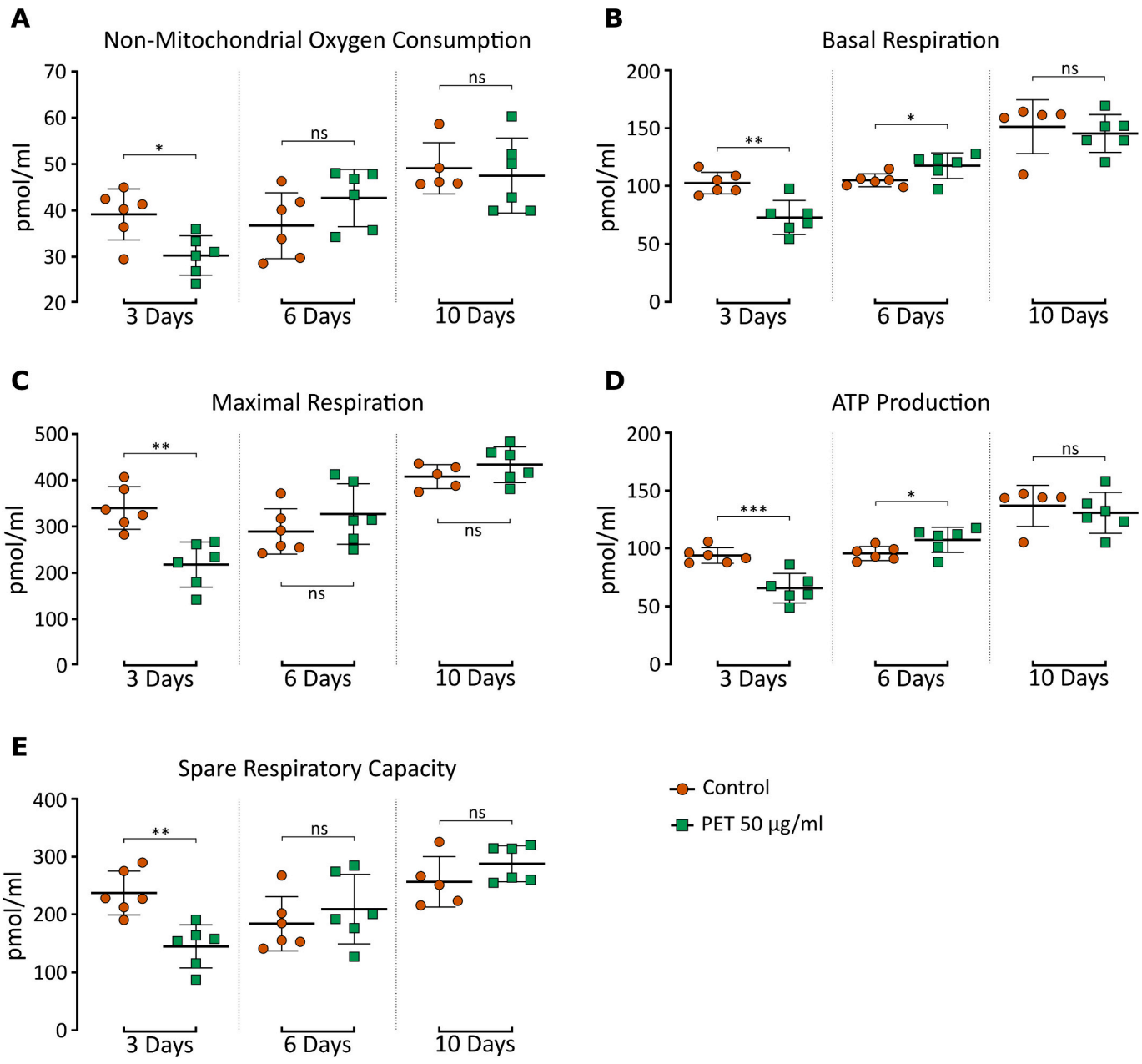

Fig. 6. Non-mitochondrial oxygen consumption (A), basal respiration (B), maximal respiration (C), ATP production (D), and spare respiratory capacity (E) activity. Control (round orange) and 50 µg/ml PET (square green) exposure for 3 days on pericytes. *$P \leq 0.05$; ** $P \leq 0.01$; ***$P \leq 0.001$. ns = non-significant. (For interpretation of the references to colour in this figure legend, the reader is referred to the web version of this article.)

However, the basal respiration ($P = 0.0323$, $F(5,5) = 3.932$, Fig. 6B) and the ATP production ($P = 0.0437$, $F(5,5) = 3.165$, Fig. 6D) are increased in pericytes exposed to PET for 6 days compared to the control group.

At day 10 exposure, there is no significant differences in all different bioenergetic measures of the mitochondrial respiration between pericytes exposed to PET or the control group, such as non-mitochondrial oxygen consumption ($P = 0.7922$, Fig. 6A), basal respiration ($P = 0.4286$, Fig. 6B), maximal respiration ($P = 0.24$, $F(5,4) = 2.210$, Fig. 6C), ATP production ($P = 0.3290$, Fig. 6D), spare respiratory capacity ($P = 0.3290$, Fig. 6E), proton leak ($P = 0.6623$, Fig. 5A), and coupling efficiency ($P = 0.6623$, Fig. 5B).

3.4. Mitochondrial copy

To assess whether PET exposure can affect the number of mitochondria of pericytes, relative mitochondrial DNA copy was measured using qPCR.

No significant difference was noted in the relative mitochondrial DNA copies between both experimental groups at 3 days ($P = 0.4964$, $F(3,3) = 7.915$), 6 days ($P = 0.3931$, $F(3,3) = 6.894$), and 10 days ($P = 0.1719$, $F(3,3) = 2.649$) exposure.

3.5. ROS level

We assessed whether PET exposure at 3, 6 and 10 days would induce changes in ROS level using the general oxidative stress indicator CM-H2DCFDA.

It is known that micro/nanoparticles may interfere with fluorescence-based assays (Ong et al., 2014). To test this potential confounding factor, the fluorescence intensity between wells containing pericyte medium were compared versus wells containing pericyte

medium with 50 µg/ml PET particles prior to the ROS assay experiment. No difference in fluorescence intensity was observed with the addition of PET particles ($P = 0.3839$, $n = 48$ per group), meaning that the fluorescence-based ROS assay selected was suitable for our purposes.

At 3 days ($P < 0.0001$, $KW = 23.58$, $n = 10$ to 20 per group), 6 days ($P < 0.0001$, $KW = 23.90$, $n = 10$ to 20 per group), and 10 days ($P < 0.0001$, $KW = 28.93$, $n = 12$ to 24 per group) exposure, pericytes do not show changes in general oxidative stress when exposed to plastic particles, but as expected, there is a significant increase of fluorescence intensity, indicating an increase of general ROS to the exposure of the positive control hydrogen peroxide (H_2O_2) prior fluorescence reading (Fig. 7).

3.6. *Expression of genes associated with oxidative stress, ferroptosis, and mitochondrial functions*

The level of expression of genes associated with oxidative stress, ferroptosis, mitochondrial functions were assessed using RT-qPCR. There was no difference of a minimum of two-fold change in the gene expression level when comparisons were drawn between the control group and the pericytes exposed for 3, 6 or 10 days to PET (Table 3).

Some of the gene expressions at 3-, 6- and 10- days were statistically significant in pericytes exposed to PET particles at 50 µg/ml compared to the control group, however the changes are still within the variation of the RT-qPCR technique, and therefore those changes are not physiologically relevant. However, it is important to note the statistical increase of *TFAM* (Table 3, Fig. 8A) and *MFN2* (Table 3, Fig. 8B) expression in pericytes exposed to PET for 6 days, especially when considering that RT-qPCR for experimental group per gene was performed on the same day, using the same master mix, and run using the same equipment, in same the same time.

4. Discussion

The aim of this study was to assess whether PET particles at 50 µg/ml would have an impact on monocultured pericyte cells in vitro. This study demonstrates that pericytes do not show signs of impaired cell viability or oxidative stress. This was indicated, respectively, by no cell viability or general ROS changes, nor changes in expression level of genes associated with oxidative stress as a result of PET nanoparticle exposure at this level for 3, 6 and 10 days. This is unexpected as cells cultured in lower concentrations of FBS, and cells that have the capability to phagocytose are more susceptible to cytotoxicity from plastic particles (Fröhlich et al., 2012). These pericytes were cultured with 2% FBS, and also have capacity to phagocytose (Winkler et al., 2014).

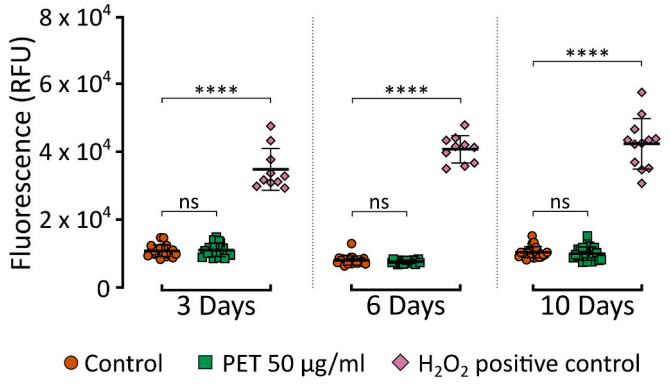

Fig. 7. Fluorescence intensity expressed in relative fluorescence units (RFU) representing general ROS expression in 3-, 6- and 10-days exposure to control (round orange), 50 µg/ml PET (square green) and H_2O_2 positive control (diamond pink) to pericytes. ns = non-significant, **** $P \leq 0.0001$. (For interpretation of the references to colour in this figure legend, the reader is referred to the web version of this article.)

Table 3
The ΔCT, standard deviation (SD), *p*, and *F* values (unpaired t-test) of gene expression (as a function of detected mRNA) levels of pericytes exposed to 50 µg/ml PET for 3, 6 and 10 days compared against untreated controls. MW = Mann-Whitney test.

Genes	Exposure time	Control ΔCT value (mean ± SD)	PET ΔCT value (mean ± SD)	*p* value	*F* (5,5) ^{A}F (4,5)
NOTCH3	3 days	5.90 ± 0.17	5.93 ± 0.12	0.7452	2.279
	6 days	5.96 ± 0.12	6.10 ± 0.14	0.0902	1.224
	10 days	0.07 ± 0.07	−0.41 ± 0.39	0.0931	MW
HIF1α	3 days	2.19 ± 0.22	1.97 ± 0.19	0.0820	1.280
	6 days	2.03 ± 0.29	2.21 ± 0.16	0.2110	3.465
	10 days	2.24 ± 0.19	2.14 ± 0.40	0.5897	4.581
SOD1	3 days	3.64 ± 0.17	4.07 ± 0.27	0.0075	2.571
	6 days	5.41 ± 0.17	5.28 ± 0.11	0.1633	2.434
	10 days	4.86 ± 0.10	4.81 ± 0.08	0.4146	1.498
GPX4	3 days	3.35 ± 0.05	3.37 ± 0.09	0.5714	2.762
	6 days	2.97 ± 0.13	3.19 ± 0.12	0.0112	1.226
	10 days	3.85 ± 0.01	3.92 ± 0.21	0.4848	MW
SLC7A11	3 days	7.90 ± 0.33	8.36 ± 0.64	0.1459	3.859
	6 days	6.61 ± 0.23	6.41 ± 0.22	0.1574	1.029
	10 days	7.21 ± 0.19	7.12 ± 0.31	0.5846	2.632
NCOA4	3 days	4.04 ± 0.08	3.96 ± 0.09	0.1158	1.172
	6 days	4.07 ± 0.18	4.21 ± 0.22	0.2515	1.511
	10 days	3.83 ± 0.13	3.97 ± 0.22	0.2232	3.112
KEAP1	3 days	5.74 ± 0.10	5.90 ± 0.07	0.0072	1.956
	6 days	6.46 ± 0.19	6.22 ± 0.18	0.0477	1.114
	10 days	5.93 ± 0.09	6.08 ± 0.22	0.0411	MW
MFN1	3 days	4.48 ± 0.06	4.36 ± 0.06	0.0075	1.142
	6 days	4.89 ± 0.10	5.00 ± 0.27	0.3845	7.739
	10 days	4.80 ± 0.15	4.86 ± 0.24	0.6536	2.614
MFN2	3 days	4.58 ± 0.10	4.62 ± 0.08	0.4782	1.537
	6 days	6.14 ± 0.31	5.65 ± 0.16	0.0059	3.779
	10 days	5.34 ± 0.08	5.65 ± 0.30	0.0354	15.27
TFAM	3 days	5.30 ± 0.15	5.05 ± 0.19	0.0304	1.740
	6 days	5.95 ± 0.12	5.54 ± 0.08	<0.0001	2.208
	10 days	5.57 ± 0.19	5.60 ± 0.35	0.8563	3.247
PINK1	3 days	7.00 ± 0.13	7.11 ± 0.20	0.2916	2.576 ^{A}
	6 days	5.21 ± 0.12	4.97 ± 0.18	0.0273	1.580
	10 days	6.18 ± 0.11	6.16 ± 0.05	0.6879	6.028
PPARGC1A	3 days	9.08 ± 0.32	9.02 ± 0.35	0.7585	1.245
	6 days	8.80 ± 0.29	9.35 ± 0.53	0.0511	3.395
	10 days	9.81 ± 0.21	9.64 ± 0.22	0.2125	1.212
NRF1	3 days	7.56 ± 0.04	7.56 ± 0.24	0.9455	28.06
	6 days	7.63 ± 0.26	7.58 ± 0.10	0.6571	6.820
	10 days	7.29 ± 0.14	7.26 ± 0.28	0.8182	MW

The targeted genes were selected for their implications in the oxidative stress pathways and ferroptosis (Li et al., 2020), which is the iron-dependant cell death connected to ROS signalling. Amongst protective signalling pathways that reduce ROS levels, oxidative stress or ferroptosis, we have selected Notch Receptor 3 (alias *NOTCH3*), which acts in a protective manner in the presence of increased ROS and ferroptosis (Li et al., 2022). Hypoxia Inducible Factor 1 Subunit Alpha (alias *HIF-1α*) (Li et al., 2019) and Superoxide Dismutase 1 (alias *SOD1*) (Eleutherio et al., 2021) were selected for their ability to reduce ROS levels and oxidative stress. Amongst genes involved in the ferroptosis pathway, we selected Glutathione Peroxidase 4 (alias *GPX4*) and Solute Carrier Family 7 Member 11 (alias *SLC7A11*), both being anti-ferroptosis biomarkers (Zuo et al., 2020) and part of the ferroptosis GSH/GPX4 pathway. Nuclear Receptor Coactivator 4 (alias *NCOA4*) and Kelch Like ECH Associated Protein 1 (alias *KEAP1*) were both selected as their function is associated with iron metabolism (Li et al., 2020) and oxidative stress (Del Rey and Mancias, 2019; Yu and Xiao, 2021).

The age of the polystyrene plastic particles influences their toxicity (Murali et al., 2015), as "aged" polystyrene nanoplastics aggregates more compared to fresh polystyrene nanoplastics and also accumulated adsorption of bioactive compounds. In this experiment, freshly

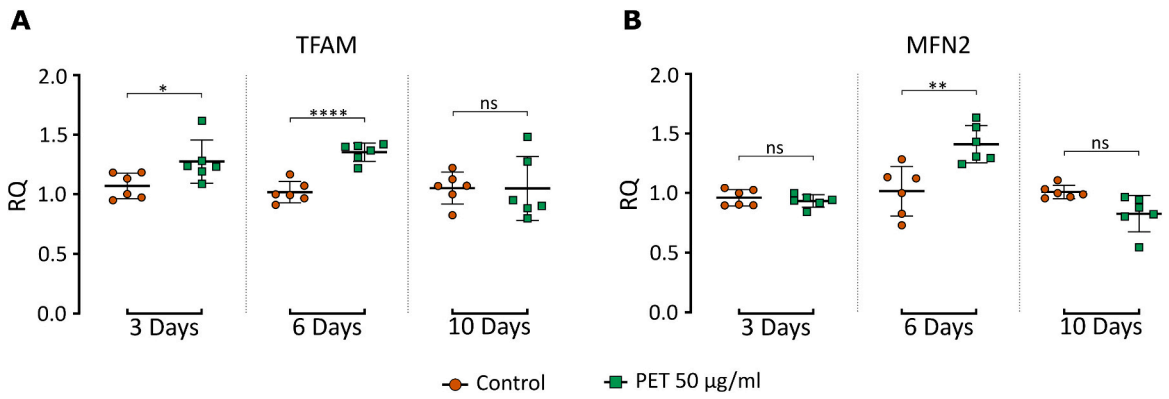

Fig. 8. Relative quantification of the fold change between control group (round orange) and the PET 50 µg/ml exposed pericytes (square green). ns = non-significant, * $P \leq 0.05$, ** $P \leq 0.01$, **** $P \leq 0.0001$. (For interpretation of the references to colour in this figure legend, the reader is referred to the web version of this article.)

generated PET particles were produced and utilised rather than "aged" PET particles (> 6 months) which may explain the lack of oxidative stress effects observed in this study.

OCR and some bioenergetics aspects of the mitochondrial functions are decreased by PET particles at 50 µg/ml exposure at day 3 but mostly return to control conditions at 6 and 10 days. ECAR measures the total acidity produced from glycolysis and the tricarboxylic acid cycle, therefore it is not possible to distinguish the exact source of the acidity. Extracellular acidification has been shown to induce ROS, leading to cell death (Teixeira et al., 2018), and we did not observe a change in either ECAR, or indications of oxidative stress at 3-, 6- and 10-days of PET exposure.

Nevertheless, our study demonstrated that pericyte mitochondrial functions adapt to a chronic stressor over time. Despite showing signs of mitochondrial dysfunctions following 3 days of exposure to PET at 50 µg/ml, the mitochondrial function of pericytes recovered by 6 days with a long-lasting effect as the recovery is still present at 10 days exposure, despite the constant presence of PET as a stressor. Interestingly, the mitochondrial functional recovery was observed by days 6 and 10 of PET particle exposure at 50 µg/ml, therefore the absence of oxidative stress may be a result of mitohormesis (Yun and Finkel, 2014) induced by PET particles.

Mitohormesis refers to the protective mechanism, by which a mild mitochondrial stressor induces a mitochondrial adaptive response to then protect the cell against future stressors. The pericyte bioenergetic recovery during chronic PET exposure suggests that there is a cellular mechanism in place to adapt, recover and maintain cellular functions, especially mitochondrial functions, despite chronic stressor insult. At day 6 of the exposure we observed a higher demand of ATP with a higher ATP production and an increase of the basal respiration suggesting a physiological adaptation (Hill et al., 2012) which may be mitohormesis in response to the stress induced by PET exposure. Conversely, despite ROS signalling being a part of the mitohormesis response (Bárcena et al., 2018), we did not observe changes of general ROS after 6- and 10-days exposure to PET, which is not surprising as ROS signalling involves a positive feedback loop which involves the reduction of ROS, while increased mitochondrial activity is maintained (Zarse et al., 2012). However, it is surprising to not observe an increase of ROS induced by 3 days exposure to PET as we observed a reduction of mitochondrial functions. It is unknown exactly at which time point the cellular mechanisms underlying the mitochondrial function recovery comes into effect, therefore the lack of general ROS change at 3 days exposure could be attributed to this recovery mechanism. Additionally, we only assessed general ROS, yet it is possible that specific ROS (Snezhkina et al., 2019) level changes due to PET exposure, but the change is masked by assessing only general ROS. Future studies examining the change in ROS levels in relation to PET particle exposure, may also benefit from more sophisticated and sensitive detection methods to investigate ROS-mediated damaged DNA and lipid or protein modifications. Also, while we did not observed changes in expression of genes associated with oxidative stress, post-transcriptional (Hernandez-Elvira and Sunnerhagen, 2022) and post-translational modifications (Cheng et al., 2023; Ebert et al., 2022; Gianazza et al., 2007; Song et al., 2023) are involved in oxidative stress response and recovery. Therefore, further study of protein modifications would be needed to investigate the mitochondrial recovery dynamics.

We investigated the expression level of genes associated with mitochondrial functions. Mitofusin 1 (alias *MFN1*) and Mitofusin 2 (alias *MFN2*) are involved in mitochondrial fusion and dynamics (Zaman and Shutt, 2022), PPARG Coactivator 1 Alpha (alias *PPARGC1A*), Nuclear Respiratory Factor 1 (alias *NRF1*) and mitochondrial transcription factor A (alias *TFAM*) are involved in mitochondrial biogenesis (Gureev et al., 2019), and PTEN Induced Kinase 1 (alias *PINK1*) is part of mitochondrial quality control (Sugiura et al., 2014).

It is interesting to note the increase of *TFAM* and *MNF2* observed in pericytes exposed to PET for 6 days. *TFAM* is known to be increased during mitohormesis (Cox et al., 2018) and can protect the mitochondrial DNA from being damaged (Lezza, 2012). Also, neuroprotective mitochondria-targeting peptide SS31, is known to increase *TFAM* and *MNF2* gene expression, as well as ATP levels (Yin et al., 2016), all of which were observed in this study following 6 days of PET exposure. Therefore, this indicates that the mitochondrial transcription factor *TFAM* would be part of the mitochondrial recovery mechanisms. There is a statistical increase of the gene *TFAM* in pericytes exposed to PET for 3 days which could indicate the premise of the increase of *TFAM* at 6 days exposure. Then at 10 days exposure, *TFAM* gene expression did not change as the mitochondrial functions recovered and stabilised. Additionally, we did not observe any increase of mitochondrial DNA copy number at any duration of exposure. It is worth noting that in other in vitro studies, an observed increase in *TFAM* expression has been determined to be insufficient to increase mitochondria DNA copy number in HeLa or HEK293 cells (Maniura-Weber et al., 2004).

Micro- and nanoplastics would not be the first toxic substance to induce mitohermesis; low dose arsenite has been shown to induce mitohormesis thus increasing lifespan (Schmeisser et al., 2013) and could potentially be linked to reduced risk of cancer (Ahn et al., 2020; Baastrup et al., 2008). However, it is important to understand at which dose PET might provide a beneficial effect via hormesis. This is because mitohormesis can be represented as a U-shaped curve where very low-doses and very high-doses of ROS are harmful but low-doses of ROS may be beneficial (Kim et al., 2018; Lee and Lee, 2019). This study only investigated a dose of PET at 50 µg/ml, while an investigation into plastic particles in human blood suggested that average plastic contamination could be as low as 1.62 µg/ml (Leslie et al., 2022), not

accounting for occupational exposure and bioaccumulation. Leslie et al. (2022) examined 22 anonymised adult donors and therefore we hypothesise that this might not reflect individuals subject to higher plastic exposures, such as occupational exposure. For instance, 3D printing has been an increasing source of concern related to indoor air pollution (Salthammer, 2022). Additionally, bioavailability and accumulation of nanoplastics in the brain is unknown - critical information that must be determined as accumulation of particle matters of diameter <1 μm could be the cause of BBB damage (Shih et al., 2018). From the BBB, the brain endothelial cells would be in direct contact to the blood supply and therefore the endothelial cells would theoretically be exposed to the plastic particle concentration as found by Leslie et al., 2022, yet we are using pericytes that wrap around the endothelial cells and are in contact with the basement membrane of the BBB. Therefore, pericytes could be exposed to fewer plastic particles than found in blood, in the context of an healthy brain, yet in the context of a damaged BBB due to previous neurotoxin exposure or disease, the accumulation of plastic particles in pericytes could be due to vulnerabilities in the BBB, allowing plastic particles to cross (Carvey et al., 2009). Therefore, we have used a higher concentration of plastic particles (50 μg/ml) in this study to consider higher plastic particle exposures and potential plastic particle accumulation at the BBB.

A subsequent set of experiments looking into lower doses of PET may reveal more findings regarding mitohormesis by focusing on studying underlying mechanisms of mitohormesis (Cheng et al., 2023). Further studies are needed to establish potential accumulations of nanoplastics in the blood brain barrier as well as the effects on the surrounding milieu, to ascertain a physiologically relevant chronic dose and to address this toxicologic hormetic dose-response relationship (Calabrese, 2005). Additionally, it is important to established whether plastic particles could damage the BBB, thereby impacting its permeability. For instance, neurotoxins involved in Parkinson's disease – such as paraquat and rotenone, – are known to induce BBB punctures creating leaks and thereby allow substances into the brain that normally would not cross the BBB (Carvey et al., 2009).

The choice of plastics and concentrations must be evaluated and considered. Ready-to-use nano and microplastics suspensions are smooth rather than being rough surfaced which does not correspond to realistic human exposure (de Sá et al., 2018). Additionally, such particles can contain additive agents that can induce toxic activity on their own and the high concentration of plastic particles used in in vitro studies can interfere with the cell medium and reduce the viability of cells grown in culture (Stock et al., 2022). This raises the question of whether plastic particles or organic additives to the plastics are more of a health concern. For instance, it has been recently shown that the additive compounds used with plastics can be more cytotoxic than the microplastic particles; however, this is dependent on size and surface charge. Stock et al. (2022) demonstrated that the cytotoxicity and cellular uptake of nanoplastics correlated directly with their size and surface charge, where smaller nanoparticles were taken up quicker and were more cytotoxic. In our study, we confirmed that we produced high purity PET particles by FTIR spectroscopy, DSC, and TGA. No significant quantity of additives was apparent, as confirmed also by TGA studies. The PET particles were most likely composed of two different populations with varying molecular weights, as shown by DSC experiments. The observation of two crystalline phases of PET could be explained by the methods used to make plastic particles from PET jars, which included grinding, milling and sieving techniques under different temperature ranges (room temperature, dry ice, liquid nitrogen).

This in vitro study aimed at focusing on the effect of plastic particles directly on pericyte cells only. The impact of nanoplastic particles on the blood-brain-barrier, nor the interplay of pericytes with other cell types to carry out their complex functions, was investigated. For example, impaired pericytes reduce the blood-brain barrier function and induce toxin accumulation in the brain (Bell et al., 2010). Therefore, more studies are needed to understand the effects of nanoplastic particles on the complex blood-brain barrier, e.g. using a mouse organotypic cortical culture (Bendfeldt et al., 2007) or human induced pluripotent stem cell (Mesentier-Louro et al., 2023) models of the blood-brain barrier. This would help determine whether PET exposure induces similar effects across populations of different cell types involved in a healthy blood-brain-barrier. Additionally, in future studies, nanoparticle tracking analysis could provide contextual information around micro and nanoparticles, particularly regarding how nanoplastics may interact with cells and organelles in culture and proteins in suspension (Filipe et al., 2010) adding valuable information as to the fate of the micro- and nanoparticles.

5. Conclusion

This study demonstrates that in vitro monocultured human pericytes exposed to 50 μg/ml PET particles for 3 days, impairs mitochondrial functions. This is followed by a recovery of the mitochondrial functions from 6 days until the 10-day exposure timeline tested. Further research looking into the stages of mitohormesis that may be being induced is necessary to definitively claim that chronic exposure to PET particles may induce mitohormesis leading mitochondrial function recovery in human pericytes monoculture.

Subsequent experiments looking at the integrity of models of the blood-brain-barrier, as well as intercellular interactions between pericytes and other cells forming the BBB, for example endothelial cells and astrocytes, are necessary to shed light on the full capabilities of plastic particles to induce potentially toxic and impairing effects or mitohormesis. Research into the accumulation of nanoplastics in the milieu of the blood-brain-barrier would shed light on the impact of nanoparticles on the tight junctions of the endothelial cells, for example.

In summary, this investigation implicates high-purity nano and micro-PET particles as impacting mitochondrial function in monocultured human brain vascular pericytes.

CRediT authorship contribution statement

Sean M. Gettings: Writing – review & editing, Visualization, Validation, Supervision, Resources, Project administration, Methodology, Investigation, Funding acquisition, Formal analysis, Conceptualization. **William Timbury:** Writing – review & editing, Visualization, Validation, Resources, Methodology, Investigation. **Anna Dmochowska:** Writing – review & editing, Writing – original draft, Visualization, Validation, Methodology, Investigation, Formal analysis, Conceptualization. **Riddhi Sharma:** Writing – review & editing, Writing – original draft, Visualization, Validation, Resources, Methodology, Investigation. **Rebecca McGonigle:** Writing – review & editing, Writing – original draft, Methodology, Investigation. **Lewis E. MacKenzie:** Writing – review & editing, Visualization, Validation, Resources, Methodology, Investigation, Formal analysis, Conceptualization. **Guillaume Miquelard-Garnier:** Writing – review & editing, Supervision, Resources, Methodology, Conceptualization. **Nora Bourbia:** Writing – original draft, Visualization, Validation, Supervision, Resources, Project administration, Methodology, Investigation, Funding acquisition, Formal analysis, Conceptualization.

Declaration of competing interest

The authors declare that they have no known competing financial interests or personal relationships that could have appeared to influence the work reported in this paper.

Data availability

Data will be made available on request.

Acknowledgement

This study is part funded by the National Institute for Health and Care Research (NIHR) Health Protection Research Unit in Chemical and Radiation Threats and Hazards (NIHR 200922), a partnership between UK Health Security Agency and Imperial College London. The views expressed are those of the author(s) and not necessarily those of the NIHR, UK Health Security Agency or the Department of Health and Social Care.

Lewis E. MacKenzie was supported by a BBSRC Discovery Fellowship award (BB/T009268/1).

The Ecole Doctorale SMI (ED 432) is acknowledged for granting Anna Dmochowska the fellowship for her Ph.D. work.

We thank Lorna Jones (UKHSA) for her advice in the making of plastic particles. We thank Dr. Paul R. Edwards and Professor Robert W. Martin (Department of Physics, University of Strathclyde) for access to and support with STEM and SEM imaging.

References

Ahn, J., Boroje, I.J., Ferdosi, H., Kramer, Z.J., Lamm, S.H., 2020. Prostate Cancer incidence in U.S. counties and low levels of arsenic in drinking Water. Int. J. Environ. Res. Public Health 17. https://doi.org/10.3390/IJERPH17030960.

Andanson, J.M., Kazarian, S.G., 2008. In situ ATR-FTIR spectroscopy of poly(ethylene terephthalate) subjected to high-temperature methanol. Macromol. Symp. 265, 195–204. https://doi.org/10.1002/MASY.200850521.

Antoniadis, G., Paraskevopoulos, K.M., Vassiliou, A.A., Papageorgiou, G.Z., Bikiaris, D., Chrissafis, K., 2011. Nonisothermal melt-crystallization kinetics for in situ prepared poly(ethylene terephthalate)/monmorilonite (PET/OMMT). Thermochim. Acta 521, 161–169. https://doi.org/10.1016/J.TCA.2011.04.019.

Baastrup, R., Sørensen, M., Balstrøm, T., Frederiksen, K., Larsen, C.L., Tjønneland, A., Overvad, K., Raaschou-Nielsen, O., 2008. Arsenic in drinking-water and risk for cancer in Denmark. Environ. Health Perspect. 116, 231–237. https://doi.org/10.1289/EHP.10623.

Baloyannis, S.J., Baloyannis, I.S., 2012. The vascular factor in Alzheimer's disease: a study in Golgi technique and electron microscopy. J. Neurol. Sci. 322, 117–121. https://doi.org/10.1016/J.JNS.2012.07.010.

Bárcena, C., Mayoral, P., Quirós, P.M., 2018. Mitohormesis, an antiaging paradigm. Int. Rev. Cell Mol. Biol. 340, 35–77. https://doi.org/10.1016/BS.IRCMB.2018.05.002.

Bell, R.D., Winkler, E.A., Sagare, A.P., Singh, I., LaRue, B., Deane, R., Zlokovic, B.V., 2010. Pericytes control key neurovascular functions and neuronal phenotype in the adult brain and during brain aging. Neuron 68, 409–427. https://doi.org/10.1016/J.NEURON.2010.09.043.

Bendfeldt, K., Radojevic, V., Kapfhammer, J., Nitsch, C., 2007. Basic fibroblast growth factor modulates density of blood vessels and preserves tight junctions in organotypic cortical cultures of mice: a new in vitro model of the blood–brain barrier. J. Neurosci. 27, 3260–3267. https://doi.org/10.1523/JNEUROSCI.4033-06.2007.

Calabrese, E.J., 2005. Paradigm lost, paradigm found: the re-emergence of hormesis as a fundamental dose response model in the toxicological sciences. Environ. Pollut. 138, 378–411. https://doi.org/10.1016/J.ENVPOL.2004.10.001.

Carvey, P.M., Hendey, B., Monahan, A.J., 2009. The blood brain barrier in neurodegenerative disease: a rhetorical perspective. J. Neurochem. 111, 291. https://doi.org/10.1111/J.1471-4159.2009.06319.X.

Chen, Q., Yin, D., Jia, Y., Schiwy, S., Legradi, J., Yang, S., Hollert, H., 2017. Enhanced uptake of BPA in the presence of nanoplastics can lead to neurotoxic effects in adult zebrafish. Sci. Total Environ. 609, 1312–1321. https://doi.org/10.1016/J.SCITOTENV.2017.07.144.

Cheng, Y.W., Liu, J., Finkel, T., 2023. Mitohormesis. Cell Metab. 35, 1872–1886. https://doi.org/10.1016/J.CMET.2023.10.011.

Chin-Chan, M., Navarro-Yepes, J., Quintanilla-Vega, B., 2015. Environmental pollutants as risk factors for neurodegenerative disorders: Alzheimer and Parkinson diseases. Front. Cell. Neurosci. 9 https://doi.org/10.3389/FNCEL.2015.00124.

Cox, C.S., McKay, S.E., Holmbeck, M.A., Christian, B.E., Scortea, A.C., Tsay, A.J., Newman, L.E., Shadel, G.S., 2018. Mitohormesis in mice via sustained basal activation of mitochondrial and antioxidant signaling. Cell Metab. 28, 776–786.e5. https://doi.org/10.1016/J.CMET.2018.07.011.

de Sá, L.C., Oliveira, M., Ribeiro, F., Rocha, T.L., Futter, M.N., 2018. Studies of the effects of microplastics on aquatic organisms: what do we know and where should we focus our efforts in the future? Sci. Total Environ. 645, 1029–1039. https://doi.org/10.1016/J.SCITOTENV.2018.07.207.

Del Rey, M.Q., Mancias, J.D., 2019. NCOA4-mediated Ferritinophagy: a potential link to neurodegeneration. Front. Neurosci. 13 https://doi.org/10.3389/FNINS.2019.00238.

Donelli, I., Taddei, P., Smet, P.F., Poelman, D., Nierstrasz, V.A., Freddi, G., 2009. Enzymatic surface modification and functionalization of PET: a water contact angle, FTIR, and fluorescence spectroscopy study. Biotechnol. Bioeng. 103, 845–856. https://doi.org/10.1002/BIT.22316.

Ebert, T., Tran, N., Schurgers, L., Stenvinkel, P., Shiels, P.G., 2022. Ageing – oxidative stress, PTMs and disease. Mol. Aspects Med. 86, 101099 https://doi.org/10.1016/J.MAM.2022.101099.

Eleutherio, E.C.A., Silva Magalhães, R.S., de Araújo Brasil, A., Monteiro Neto, J.R., de Holanda Paranhos, L., 2021. SOD1, more than just an antioxidant. Arch. Biochem. Biophys. 697, 108701 https://doi.org/10.1016/J.ABB.2020.108701.

Fávaro, S.L., Rubira, A.F., Muniz, E.C., Radovanovic, E., 2007. Surface modification of HDPE, PP, and PET films with KMnO4/HCl solutions. Polym. Degrad. Stab. 92, 1219–1226. https://doi.org/10.1016/J.POLYMDEGRADSTAB.2007.04.005.

Filipe, V., Hawe, A., Jiskoot, W., 2010. Critical evaluation of nanoparticle tracking analysis (NTA) by NanoSight for the measurement of nanoparticles and protein aggregates. Pharm. Res. 27, 796–810. https://doi.org/10.1007/S11095-010-0073-2.

Fröhlich, E., Meindl, C., Roblegg, E., Griesbacher, A., Pieber, T.R., 2012. Cytotoxity of nanoparticles is influenced by size, proliferation and embryonic origin of the cells used for testing. Nanotoxicology 6, 424–439. https://doi.org/10.3109/17435390.2011.586478.

Gianazza, E., Crawford, J., Miller, I., 2007. Detecting oxidative post-translational modifications in proteins. Amino Acids 33, 51–56. https://doi.org/10.1007/S00726-006-0410-2.

Gureev, A.P., Shaforostova, E.A., Popov, V.N., 2019. Regulation of mitochondrial biogenesis as a way for active longevity: interaction between the Nrf2 and PGC-1α signaling pathways. Front. Genet. 10 https://doi.org/10.3389/FGENE.2019.00435.

Halliday, M.R., Rege, S.V., Ma, Q., Zhao, Z., Miller, C.A., Winkler, E.A., Zlokovic, B.V., 2016. Accelerated pericyte degeneration and blood–brain barrier breakdown in apolipoprotein E4 carriers with Alzheimer's disease. J. Cereb. Blood Flow Metab. 36, 216. https://doi.org/10.1038/JCBFM.2015.44.

Han, Z., Wang, Yao, Wang, J., Wang, S., Zhuang, H., Liu, J., Huang, L., Wang, Yanxin, Wang, W., Belfiore, L.A., Tang, J., 2018. Preparation of hybrid nanoparticle nucleating agents and their effects on the crystallization behavior of poly(ethylene terephthalate). Mater 11, 587, 11. 587. https://doi.org/10.3390/MA11040587.

Hartmann, N.B., Hüffer, T., Thompson, R.C., Hassellöv, M., Verschoor, A., Daugaard, A. E., Rist, S., Karlsson, T., Brennholt, N., Cole, M., Herrling, M.P., Hess, M.C., Ivleva, N. P., Lusher, A.L., Wagner, M., 2019. Are we speaking the same language? Recommendations for a definition and categorization framework for plastic debris. Environ. Sci. Technol. 53, 1039–1047. https://doi.org/10.1021/ACS.EST.8B05297.

Heintzmann, R., Ficz, G., 2006. Breaking the resolution limit in light microscopy. Brief. Funct. Genomics 5, 289–301. https://doi.org/10.1093/BFGP/ELL036.

Hernandez-Elvira, M., Sunnerhagen, P., 2022. Post-transcriptional regulation during stress. FEMS Yeast Res. 22, 1–11. https://doi.org/10.1093/FEMSYR/FOAC025.

Hill, B.G., Benavides, G.A., Lancaster, J.J.R., Ballinger, S., Dell'Italia, L., Zhang, J., Darley-Usmar, V.M., 2012. Integration of cellular bioenergetics with mitochondrial quality control and autophagy. Biol. Chem. 393, 1485–1512. https://doi.org/10.1515/HSZ-2012-0198.

Hoelting, L., Scheinhardt, B., Bondarenko, O., Schildknecht, S., Kapitza, M., Tanavde, V., Tan, B., Lee, Q.Y., Mecking, S., Leist, M., Kadereit, S., 2013. A 3-dimensional human embryonic stem cell (hESC)-derived model to detect developmental neurotoxicity of nanoparticles. Arch. Toxicol. 87, 721–733. https://doi.org/10.1007/S00204-012-0984-2.

Hussain, K.A., Romanova, S., Okur, I., Zhang, D., Kuebler, J., Huang, X., Wang, B., Fernandez-Ballester, L., Lu, Y., Schubert, M., Li, Y., 2023. Assessing the release of microplastics and Nanoplastics from plastic containers and reusable food pouches: implications for human health. Environ. Sci. Technol. 57, 9782–9792. https://doi.org/10.1021/ACS.EST.3C01942.

Jadhav, E.B., Sankhla, M.S., Bhat, R.A., Bhagat, D.S., 2021. Microplastics from food packaging: an overview of human consumption, health threats, and alternative solutions. Environ. Nanotechnology, Monit. Manag. 16, 100608 https://doi.org/10.1016/J.ENMM.2021.100608.

Jenner, L.C., Rotchell, J.M., Bennett, R.T., Cowen, M., Tentzeris, V., Sadofsky, L.R., 2022. Detection of microplastics in human lung tissue using μFTIR spectroscopy. Sci. Total Environ. 831, 154907 https://doi.org/10.1016/J.SCITOTENV.2022.154907.

Ji, Y., Wang, C., Wang, Y., Fu, L., Man, M., Chen, L., 2020. Realistic polyethylene terephthalate nanoplastics and the size- and surface coating-dependent toxicological impacts on zebrafish embryos. Environ. Sci. Nano 7, 2313–2324. https://doi.org/10.1039/D0EN00464B.

Kim, S.A., Lee, Y.M., Choi, J.Y., Jacobs, D.R., Lee, D.H., 2018. Evolutionarily adapted hormesis-inducing stressors can be a practical solution to mitigate harmful effects of chronic exposure to low dose chemical mixtures. Environ. Pollut. 233, 725–734. https://doi.org/10.1016/J.ENVPOL.2017.10.124.

Kopatz, V., Wen, K., Kovács, T., Keimowitz, A.S., Pichler, V., Widder, J., Vethaak, A.D., Hollóczki, O., Kenner, L., 2023. Micro- and nanoplastics breach the blood–brain barrier (BBB): biomolecular corona's role revealed. Nanomater 13, 1404, 13. https://doi.org/10.3390/NANO13081404.

Kriit, H.K., Forsberg, B., Åström, D.O., Oudin, A., 2021. Annual dementia incidence and monetary burden attributable to fine particulate matter (PM2.5) exposure in Sweden. Environ. Heal. A Glob. Access Sci. Source 20, 1–12. https://doi.org/10.1186/S12940-021-00750-X.

Landrigan, P.J., Stegeman, J.J., Fleming, L.E., Allemand, D., Anderson, D.M., Backer, L. C., Brucker-Davis, F., Chevalier, N., Corra, L., Czerucka, D., Bottein, M.Y.D., Demeneix, B., Depledge, M., Deheyn, D.D., Dorman, C.J., Fénichel, P., Fisher, S., Gaill, F., Galgani, F., Gaze, W.H., Giuliano, L., Grandjean, P., Hahn, M.E., Hamdoun, A., Hess, P., Judson, B., Laborde, A., McGlade, J., Mu, J., Mustapha, A., Neira, M., Noble, R.T., Pedrotti, M.L., Reddy, C., Rocklöv, J., Scharler, U.M., Shanmugam, H., Taghian, G., Van De Water, J.A.J.M., Vezzulli, L., Weihe, P., Zeka, A., Raps, H., Rampal, P., 2020. Human health and ocean pollution. Ann. Glob. Heal. 86, 1–64. https://doi.org/10.5334/AOGH.2831.

Lee, Y.M., Lee, D.H., 2019. Mitochondrial toxins and healthy lifestyle meet at the crossroad of Hormesis. Diabetes Metab. J. 43, 568. https://doi.org/10.4093/DMJ.2019.0143.

Lei, L., Liu, M., Song, Y., Lu, S., Hu, J., Cao, C., Xie, B., Shi, H., He, D., 2018. Polystyrene (nano)microplastics cause size-dependent neurotoxicity, oxidative damage and other adverse effects in Caenorhabditis elegans. Environ. Sci. Nano 5, 2009–2020. https://doi.org/10.1039/C8EN00412A.

Lendahl, U., Nilsson, P., Betsholtz, C., 2019. Emerging links between cerebrovascular and neurodegenerative diseases—a special role for pericytes. EMBO Rep. 20 https://doi.org/10.15252/EMBR.201948070.

Leslie, H.A., van Velzen, M.J.M., Brandsma, S.H., Vethaak, A.D., Garcia-Vallejo, J.J., Lamoree, M.H., 2022. Discovery and quantification of plastic particle pollution in human blood. Environ. Int. 163 https://doi.org/10.1016/J.ENVINT.2022.107199.

Lezza, A.M.S., 2012. Mitochondrial transcription factor a (TFAM): one actor for different roles. Front. Biol. (Beijing). 7, 30–39. https://doi.org/10.1007/S11515-011-1175-X.

Li, H.S., Zhou, Y.N., Li, L., Li, S.F., Long, D., Chen, X.L., Zhang, J.B., Feng, L., Li, Y.P., 2019. HIF-1α protects against oxidative stress by directly targeting mitochondria. Redox Biol. 25 https://doi.org/10.1016/J.REDOX.2019.101109.

Li, J., Cao, F., Yin, H., Jian, Z., Lin, Z. Tao, Mao, N., Sun, B., Wang, G., 2020. Ferroptosis: past, present and future. Cell Death Dis. 11 https://doi.org/10.1038/S41419-020-2298-2.

Li, Z., Xiao, J.Y., Liu, M., Cui, J., Lian, B., Sun, Y., Li, C., 2022. Notch3 regulates ferroptosis via ROS-induced lipid peroxidation in NSCLC cells. FEBS Open Bio 12, 1197–1205. https://doi.org/10.1002/2211-5463.13393.

Liu, Q., Chen, Z., Chen, Y., Yang, F., Yao, W., Xie, Y., 2021. Microplastics and Nanoplastics: emerging contaminants in food. J. Agric. Food Chem. 69, 10450–10468. https://doi.org/10.1021/ACS.JAFC.1C04199.

Maniura-Weber, K., Goffart, S., Garstka, H.L., Montoya, J., Wiesner, R.J., 2004. Transient overexpression of mitochondrial transcription factor a (TFAM) is sufficient to stimulate mitochondrial DNA transcription, but not sufficient to increase mtDNA copy number in cultured cells. Nucleic Acids Res. 32, 6015–6027. https://doi.org/10.1093/NAR/GKH921.

Mattsson, K., Johnson, E.V., Malmendal, A., Linse, S., Hansson, L.A., Cedervall, T., 2017. Brain damage and behavioural disorders in fish induced by plastic nanoparticles delivered through the food chain. Sci. Reports 71 (7), 1–7. https://doi.org/10.1038/s41598-017-10813-0.

Mesentier-Louro, L.A., Suhy, N., Broekaart, D., Bula, M., Pereira, A.C., Blanchard, J.W., 2023. Modeling the blood-brain barrier using human-induced pluripotent stem cells. Methods Mol. Biol. 2683, 135–151. https://doi.org/10.1007/978-1-0716-3287-1_11.

Murali, K., Kenesei, K., Li, Y., Demeter, K., Környei, Z., Madarász, E., 2015. Uptake and bio-reactivity of polystyrene nanoparticles is affected by surface modifications, ageing and LPS adsorption: in vitro studies on neural tissue cells. Nanoscale 7, 4199–4210. https://doi.org/10.1039/C4NR06849A.

Ong, K.J., MacCormack, T.J., Clark, R.J., Ede, J.D., Ortega, V.A., Felix, L.C., Dang, M.K. M., Ma, G., Fenniri, H., Veinot, J.G.C., Goss, G.G., 2014. Widespread nanoparticle-assay interference: implications for Nanotoxicity testing. PloS One 9, e90650. https://doi.org/10.1371/JOURNAL.PONE.0090650.

Prüst, M., Meijer, J., Westerink, R.H.S., 2020. The plastic brain: neurotoxicity of micro- and nanoplastics. Part. Fibre Toxicol. 171, 1–16. https://doi.org/10.1186/S12989-020-00358-Y.

Quaegebeur, A., Segura, I., Carmeliet, P., 2010. Pericytes: blood-brain barrier safeguards against neurodegeneration? Neuron 68, 321–323. https://doi.org/10.1016/J.NEURON.2010.10.024.

Ragusa, A., Svelato, A., Santacroce, C., Catalano, P., Notarstefano, V., Carnevali, O., Papa, F., Rongioletti, M.C.A., Baiocco, F., Draghi, S., D'Amore, E., Rinaldo, D., Matta, M., Giorgini, E., 2021. Plasticenta: first evidence of microplastics in human placenta. Environ. Int. 146, 106274 https://doi.org/10.1016/J.ENVINT.2020.106274.

Ragusa, A., Notarstefano, V., Svelato, A., Belloni, A., Gioacchini, G., Blondeel, C., Zucchelli, E., De Luca, C., D'avino, S., Gulotta, A., Carnevali, O., Giorgini, E., 2022. Raman microspectroscopy detection and characterisation of microplastics in human breastmilk. Polymers (Basel). 14 https://doi.org/10.3390/POLYM14132700.

Rooney, J.P., Ryde, I.T., Sanders, L.H., Howlett, E.V., Colton, M.D., Germ, K.E., Mayer, G. D., Timothy Greenamyre, J., Meyer, J.N., 2015. PCR based determination of mitochondrial DNA copy number in multiple species. Methods Mol. Biol. 1241, 23. https://doi.org/10.1007/978-1-4939-1875-1_3.

Salthammer, T., 2022. Microplastics and their additives in the indoor environment. Angew. Chem. Int. Ed. Engl. 61 https://doi.org/10.1002/ANIE.202205713, 202205713.

Schirinzi, G.F., Pérez-Pomeda, I., Sanchís, J., Rossini, C., Farré, M., Barceló, D., 2017. Cytotoxic effects of commonly used nanomaterials and microplastics on cerebral and epithelial human cells. Environ. Res. 159, 579–587. https://doi.org/10.1016/J.ENVRES.2017.08.043.

Schmeisser, S., Schmeisser, K., Weimer, S., Groth, M., Priebe, S., Fazius, E., Kuhlow, D., Pick, D., Einax, J.W., Guthke, R., Platzer, M., Zarse, K., Ristow, M., 2013. Mitochondrial hormesis links low-dose arsenite exposure to lifespan extension. Aging Cell 12, 508. https://doi.org/10.1111/ACEL.12076.

Schneider, C.A., Rasband, W.S., Eliceiri, K.W., 2012. NIH image to ImageJ: 25 years of image analysis. Nat. Methods 97, 671–675. https://doi.org/10.1038/nmeth.2089, 9.

Shih, C.H., Chen, J.K., Kuo, L.W., Cho, K.H., Hsiao, T.C., Lin, Z.W., Lin, Y.S., Kang, J.H., Lo, Y.C., Chuang, K.J., Cheng, T.J., Chuang, H.C., 2018. Chronic pulmonary exposure to traffic-related fine particulate matter causes brain impairment in adult rats. Part. Fibre Toxicol. 15, 1–17. https://doi.org/10.1186/S12989-018-0281-1.

Snezhkina, A.V., Kudryavtseva, A.V., Kardymon, O.L., Savvateeva, M.V., Melnikova, N. V., Krasnov, G.S., Dmitriev, A.A., 2019. ROS generation and antioxidant defense Systems in Normal and Malignant Cells. Oxid. Med. Cell. Longev. 2019 https://doi.org/10.1155/2019/6175804.

Song, Y., Qu, Y., Mao, C., Zhang, R., Jiang, D., Sun, X., 2023. Post-translational modifications of Keap1: the state of the art. Front. Cell Dev. Biol. 11, 1332049. https://doi.org/10.3389/FCELL.2023.1332049/.

Stock, V., Böhmert, L., Coban, G., Tyra, G., Vollbrecht, M.L., Voss, L., Paul, M.B., Braeuning, A., Sieg, H., 2022. Microplastics and nanoplastics: size, surface and dispersant – what causes the effect? Toxicol. Vitr. 80, 105314 https://doi.org/10.1016/J.TIV.2022.105314.

Sugiura, A., McLelland, G.-L., Fon, E.A., McBride, H.M., 2014. A new pathway for mitochondrial quality control: mitochondrial-derived vesicles. EMBO J. 33, 2142. https://doi.org/10.15252/EMBJ.201488104.

Teixeira, J., Basit, F., Swarts, H.G., Forkink, M., Oliveira, P.J., Willems, P.H.G.M., Koopman, W.J.H., 2018. Extracellular acidification induces ROS- and mPTP-mediated death in HEK293 cells. Redox Biol. 15, 394–404. https://doi.org/10.1016/J.REDOX.2017.12.018.

Winkler, E.A., Sagare, A.P., Zlokovic, B.V., 2014. The Pericyte: a forgotten cell type with important implications for Alzheimer's disease? Brain Pathol. 24, 371. https://doi.org/10.1111/BPA.12152.

Yang, Y., Xie, E., Du, Z., Peng, Z., Han, Z., Li, L., Zhao, R., Qin, Y., Xue, M., Li, F., Hua, K., Yang, X., 2023. Detection of various microplastics in patients undergoing cardiac surgery. Environ. Sci. Technol. https://doi.org/10.1021/ACS.EST.2C07179.

Yin, X., Manczak, M., Reddy, P.H., 2016. Mitochondria-targeted molecules MitoQ and SS31 reduce mutant huntingtin-induced mitochondrial toxicity and synaptic damage in Huntington's disease. Hum. Mol. Genet. 25, 1739. https://doi.org/10.1093/HMG/DDW045.

Yu, C., Xiao, J.H., 2021. The Keap1-Nrf2 system: a mediator between oxidative stress and aging. Oxid. Med. Cell. Longev. 2021 https://doi.org/10.1155/2021/6635460.

Yun, J., Finkel, T., 2014. Mitohormesis. Cell Metab. 19, 757–766. https://doi.org/10.1016/J.CMET.2014.01.011.

Zaman, M., Shutt, T.E., 2022. The role of impaired mitochondrial dynamics in MFN2-mediated pathology. Front. Cell Dev. Biol. 10, 858286 https://doi.org/10.3389/FCELL.2022.858286.

Zarse, K., Schmeisser, S., Groth, M., Priebe, S., Beuster, G., Kuhlow, D., Guthke, R., Platzer, M., Kahn, C.R., Ristow, M., 2012. Impaired insulin/IGF1 signaling extends life span by promoting mitochondrial L-proline catabolism to induce a transient ROS signal. Cell Metab. 15, 451–465. https://doi.org/10.1016/J.CMET.2012.02.013.

Zhang, B., Chao, J., Chen, L., Liu, L., Yang, X., Wang, Q., 2021. Research progress of nanoplastics in freshwater. Sci. Total Environ. 757 https://doi.org/10.1016/J.SCITOTENV.2020.143791.

Zuo, S., Yu, J., Pan, H., Lu, L., 2020. Novel insights on targeting ferroptosis in cancer therapy. Biomark. Res. 81, 1–11. https://doi.org/10.1186/S40364-020-00229-W.